A Single-Phase Grid-Connected Photovoltaic Power System using DFCM Converter

Farzam Baradarani, Seyed Hossein Hosseini, and Farzam Nejabatkhah

Department of Electrical and Computer Engineering, University of Tabriz, Tabriz, Iran
baradarani.f@gmail.com, hosseini@tabrizu.ac.ir, farzamnejabatkhah@gmail.com

Abstract

This paper presents a single-phase grid-connected photovoltaic power system with the capability of maximum power point tracking (MPPT) of photovoltaic (PV) array and reactive power compensation. This topology employs a boost converter to track the maximum power point of PV array and a dual flying capacitor multicell (DFCM) converter in order to connect to the grid. The proposed system can fulfill comprehensive reactive power performance even when the PV power is unavailable. The four-cell nine-level DFCM converter, controlled with modified PSPWM, has improved output voltage frequency spectrum, and low harmonic distortion with reduced number of switches among nine-level inverters. The simulation results, developed in MATLAB software, verify the performance and advantages of the proposed system.

1. Introduction

Renewable energy is a challenging aspect for now and future of the world's increasing energy demand. Since last three decades, there is a growing effort to make renewable energy more feasible due to its particular characteristics and high costs. Among renewable energy sources, photovoltaic energy is one of the most considerable sources because of its advantages like being widely available and cost free, clean and abundant. Furthermore, being a semiconductor device it is free of moving parts which results little operation and maintenance costs [1]. The PV model has been described and developed in several literatures due to necessity of an accurate model in computer simulations [1, 2, 3, 4]. To connect the PV array to the utility grid, power electronic converters carry out a prominent role, i.e., tracking the maximum power point of the PV array, injecting a sinusoidal current to the grid, and even power conditioning.

A comprehensive discussion about single-phase grid-connected PV system with power conditioning capability has been given in [7, 8]. Multilevel converters are proper alternatives for medium and high power applications and possess some advantages like increased number of output voltage levels, which improves output voltage spectrum with low harmonic distortion and reduces filter requirements. The inverter used in this paper is dual flying capacitor multicell (DFCM) converter [9]. Although high number of semiconductors and capacitors is a matter of concern in multilevel inverters, it has been improved in DFCM converter. Some topologies of converters for single phase grid-connected PV systems investigated in [10, 11, 12]. The proposed topology uses a boost converter at first stage to track the maximum power point of the PV array and boost the PV voltage to a sufficient level to connect to the grid. At second stage the DFCM converter, converts the proper DC voltage to grid synchronous AC voltage.

Table 1. PV model parameters

Parameters	Description	Unit
I	Model output current	A
I_{PH}	Photovoltaic current	A
I_D	Model diode current	A
I_{SH}	Model shunt resistance current	A
I_{sat}	Model diode saturation current	A
T_c	Solar cell temperature	$Kelvin$
T_a	Ambient temperature	$Kelvin$
G_a	Ambient irradiation	W/m^2
T_{cSTC}	PV panel STC temperature	K
G_{aSTC}	PV panel STC irradiation	W/m^2
I_{scSTC}	PV short circuit current at STC	$8.15\ A$
C_2	Coefficient	$0.03\ K.m^2/W$
α	Temperature coefficient of short circuit current	0.0033
V_{ocSTC}	PV open circuit voltage at STC	$29.4\ V$
β	Temperature coefficient of open circuit voltage	$-2.3 \times 10^{-3}\ V/K$
q	Electron charge	$1.602 \times 10^{-19}\ C$
K	Boltzmann constant	$1.381 \times 10^{-23}\ J/K$
n	Diode ideality factor	1.3
V_g	PV material band gap voltage	$1.12\ V$
N_s	No. of series solar cells	48
R_s	Model series resistance	Ω
R_{SH}	Model shunt resistance	Ω

The load angle is variable and determines the reactive power flow direction between the proposed system and grid to compensate reactive power. This system is suitable for distribution networks that suffer from poor power quality and voltage sags injecting active and reactive power to the network.

2. PV Model

The PV model used in this paper is based on the equivalent circuit shown in Fig. 1. This model accepts ambient temperature and irradiation level as input parameters and calculates the PV output current as a function of its terminal voltage [2, 3]. The standard test conditions (STC) of the PV array is $T_{cSTC} = 298.15°K$ and $G_{aSTC} = 1000\,W/m^2$. From the equivalent circuit, the current equation is obtained as follows (parameters of the equations are listed in Table 1):

$$I = I_{PH} - I_D - I_{SH} \tag{1}$$

where I_{PH}, I_D, and I_{SH} can be written as:

$$I_{PH} = \left[1 + \alpha \times \frac{T_c - T_{cSTC}}{I_{scSTC}}\right] \times I_{scSTC} \times \frac{G_a}{G_{aSTC}} \tag{2}$$

$$I_D = I_{sat} \times (e^{\frac{q(V+IR_S)}{nkT_cN_s}} - 1) \tag{3}$$

$$I_{SH} = \frac{V+IR_s}{R_{SH}} \tag{4}$$

in the above equations, I_{sat} and T_c can be represented as:

$$T_c = T_a + C_2 G_a \tag{5}$$

$$I_{sat} = \frac{I_{scSTC}}{\left(e^{\frac{qV_{ocSTC}}{nkT_{cSTC}N_s}}-1\right)} \times \left(\frac{T_c}{T_{cSTC}}\right)^{\frac{3}{n}} \times e^{-\frac{qV_g}{nk}\times\left(\frac{1}{T_c}-\frac{1}{T_{cSTC}}\right)} \tag{6}$$

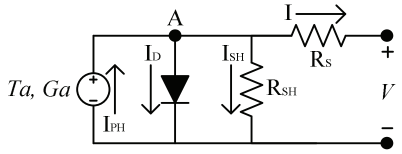

Fig. 1. Equivalent circuit of PV cell

by substituting (2)-(6) in (1), I can be written as:

$$I = \left[1 + \alpha \times \frac{T_c - T_{cSTC}}{I_{scSTC}}\right] \times I_{scSTC} \times \frac{G_a}{G_{aSTC}} - \frac{I_{scSTC}}{\left(e^{\frac{qV_{ocSTC}}{nkT_{cSTC}N_s}}-1\right)} \times \left(\frac{T_c}{T_{cSTC}}\right)^{\frac{3}{n}} \times e^{-\frac{qV_g}{nk}\times\left(\frac{1}{T_c}-\frac{1}{T_{cSTC}}\right)} \times \left(e^{\frac{q(V+IR_s)}{nkT_cN_s}} - 1\right) - \frac{V+IR_s}{R_{SH}} \tag{7}$$

Equation (7) is non-linear, so it only can be solved using numerical methods which are time consuming during simulation. However, we can use simplified PV model by eliminating the series and shunt resistances in the PV equivalent circuit that is commonly neglected. This assumption results ideal model for PV cells and linear I-V equation. For an ideal PV cell there is no series loss and no leakage current to ground [1, 4]. Therefore, the linear output PV current can be determined as:

$$I = \left[1 + \alpha \times \frac{T_c - T_{cSTC}}{I_{scSTC}}\right] \times I_{scSTC} \times \frac{G_a}{G_{aSTC}} - \frac{I_{scSTC}}{\left(e^{\frac{qV_{ocSTC}}{nkT_{cSTC}N_s}}-1\right)} \times \left(\frac{T_c}{T_{cSTC}}\right)^{\frac{3}{n}} \times e^{-\frac{qV_g}{nk}\times\left(\frac{1}{T_c}-\frac{1}{T_{cSTC}}\right)} \times \left(e^{\frac{qV}{nkT_cN_s}} - 1\right) \tag{8}$$

In this paper, the PV module is modeled in the MATLAB software based on (8).

3. DFCM Converter

The main advantages of multicell converters can be aggregate into the followings [9, 10]:

- Suitable for medium and high power applications
- High number of output voltage levels
- Improved output voltage frequency spectrum
- Low harmonic distortion
- Reduced filter requirements
- Transformerless operation
- Naturally balancing of the flying capacitor voltages

The DFCM converter include all aforementioned advantages with 50% reduction of number of high frequency switches, flying capacitors, and DC sources in comparison with flying capacitor multicell (FCM) and stacked multicell (SM) converters. Besides, in comparison with cascaded multicell (CM) converter, the DFCM converter has reduced number of high frequency switches by 50% and DC sources by $\frac{100}{n}$% (n is the number of cells).

The DFCM converter is constructed by adding only two low-frequency switches to the conventional configuration of FCM converter while the number of high-frequency switches and capacitors, voltage ratings of capacitors and switches, and the number of high-frequency switching during a full cycle are kept constant. Table 2 compares CM, FCM, SM, and DFCM converters for the identical output voltage with equal number of levels ($2n$+1). DFCM converter schematic diagram is shown in Fig. 3 [9].

Table 2. Comparison between CM, FCM, SM and DFCM for the same output voltage

Type of multicell converter	No. of high frequency switches	No. of low frequency switches	No. of Capacitors	No. of DC sources
CM	4n	0	0	n
FCM	4n	0	2n-1	2
SM	4n	0	2n-2	2
DFCM	2n	2	n-1	1

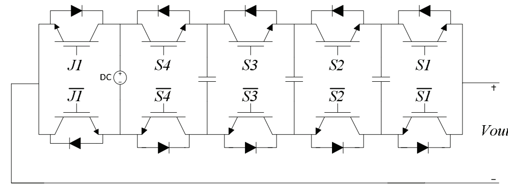

Fig. 3. Schematic diagram of DFCM converter

4. Proposed System Configuration

Fig. 4 shows the proposed system schematic/block diagram. Output terminal of the PV array is connected to the grid through two stages of power conversion. First stage is a boost converter which is considered to track maximum power point of the PV array and to boost the PV output voltage. The DFCM converter is utilized in the second stage in order to invert DC voltage to the grid synchronous AC voltage and control the system's active and reactive power. Natural balancing boost filter is recommended during transient conditions. This filter consists of two RLC filters that accelerates self-balancing property of the flying capacitors voltages and connects in parallel with the grid (or load). These two filters are tuned to f_{sw} and $2f_{sw}$ where f_{sw} is the DFCM switching frequency [9]. The natural balancing boost filter can be disconnected during steady state conditions due to its resistive losses. The boost and DFCM converter parameters are given in Table 3. The DFCM converter directly connects to grid and no bulky transformer is needed.

Table 3. Boost and DFCM converter parameters

Boost Converter	
Switching frequency	10 kHz
Boost Inductor	50 μH
Input and Output Capacitors	8 mF
DFCM Converter	
Switching frequency	1.5 kHz
Output RLC filter tuned to f_{sw}	0.1 Ω; 5.11 mH; 2.2 µF
Output RLC filter tuned to $2f_{sw}$	0.1 Ω; 1.27 mH; 2.2 µF
Flying Capacitors	2 mF
Output fundamental voltage frequency	50 Hz

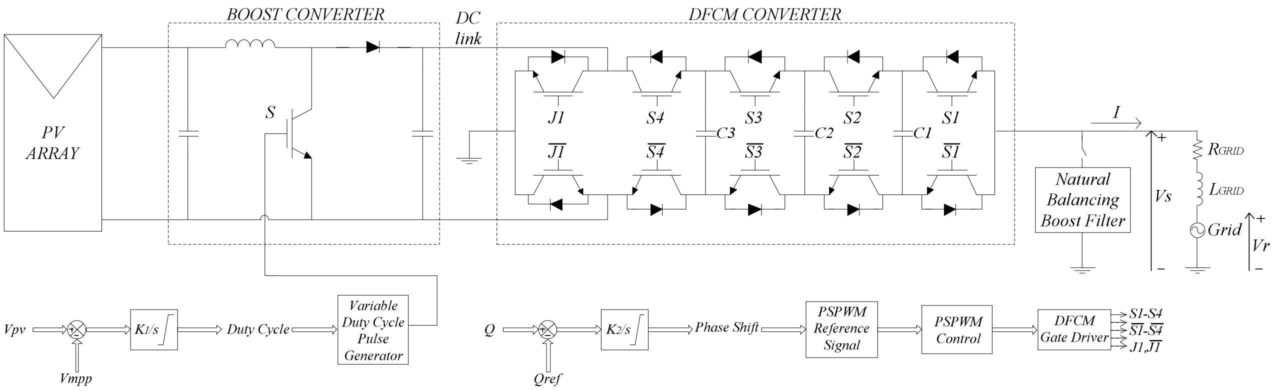

Fig. 4. Power circuit schematic diagram and control system block diagram of the proposed system

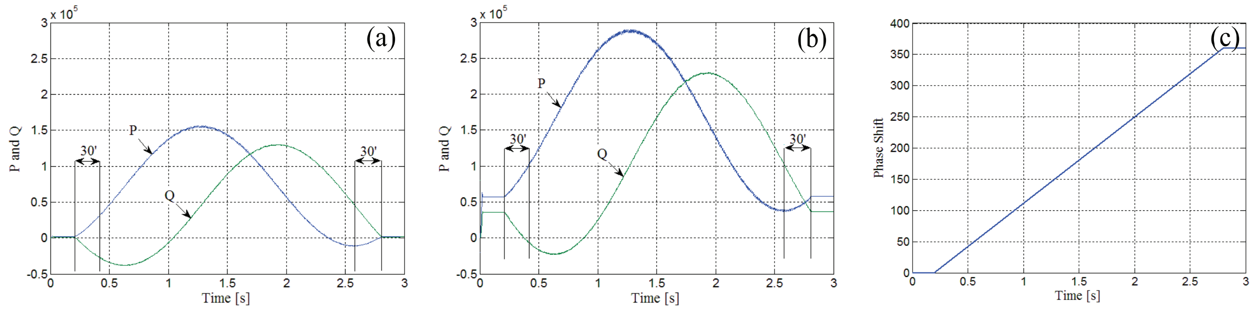

Fig. 5. P and Q exchange between the proposed system and grid, using an ideal DC voltage source instead of PV array and boost converter, (a) For 400 V DC link voltage, (b) For 600 V DC link voltage, (c) The phase shift of output voltage during simulation

5. Control System

The control system has three main features. These features are maximum power point tracking of the PV array, reactive power compensation, and modified PSPWM strategy for switching the DFCM converter. Typical algorithms such as perturbation and observation (P&O), incremental conductance (INC), parasitic capacitance (PC), and constant voltage (CV) [3, 6] are available to determine the MPP of the PV array. In this paper, constant voltage method is used.

Although any changes in output voltage phase shift (δ) or duty cycle of the boost converter (D) affects active (P) and reactive (Q) powers, in the control system of the proposed structure, P is adjusted on its reference value by D and Q is controlled by δ. The variation of P and Q are illustrated in Figs. 5(a) and 5(b) for DC link voltages of 400 and 600 from an ideal DC voltage source, while δ has been changed between 0 and 360 degrees as shown in Fig. 5(c). Obviously, the effect of duty cycle is shifting P and Q curves upwards or downwards. It means that if D is increased, P and Q both will increase.

In the control system, it is considering that δ belongs to [-30°, 30°]. In this interval, if δ is increased, P will increase but Q will decrease. These conditions are considered in the control system, which has been limited to work in the interval [-30°,30°].

Control system block diagram is shown in Fig. 4. Phase shift of the output voltage corresponds to PSPWM reference signal. Four carrier signals, each for switches of one cell, are needed and their frequency determines the switching frequency.

Switching strategy has been completely discussed in [9].

6. Simulation Results

The system performance in various conditions is verified by MATLAB software. These conditions are applied to the system by changing the irradiation level of the PV array and reactive power requirement. The PV array consists of 120 PV modules (SPG1786T-02E [2]) with a maximum output power of 20kW. Ten PV modules connected in series as a PV string and twelve of PV strings are paralleled to produce the PV array. It is worth to mention that all semiconductors are ideal. Simulation period is 2.4 seconds and consists of four stages. As mentioned previously, this system can compensate reactive power in a wide range; the only limit is the semiconductors and capacitors rating values. Q_{ref} values in this simulation are given in Table 6. Table 4 shows the time that is needed for system to perform reactive power variation. In the simulation, the grid impedance is assumed a resistive-inductive series branch with the values $R_{Grid} = 0.5\ \Omega$; $L_{Grid} = 1\ mH$. Fig. 6 illustrates active and reactive powers that are injected to the grid. The PV array output voltage and current are shown in Fig. 7. Output voltage phase shift and boost converter output voltage are depicted in Figs. 8 and 10. Moreover, Fig. 11 shows the flying capacitors voltages.

6.1. Stage 1: 0<t<0.6

This stage starts with system initial condition. All capacitors initial voltages are zero. It takes 0.2 sec for both DC link

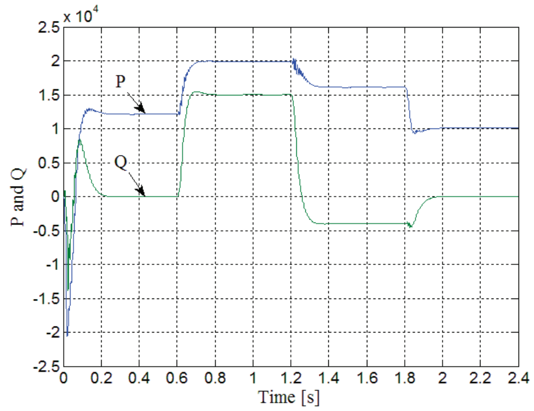

Fig. 6. Active and reactive power injected to the grid

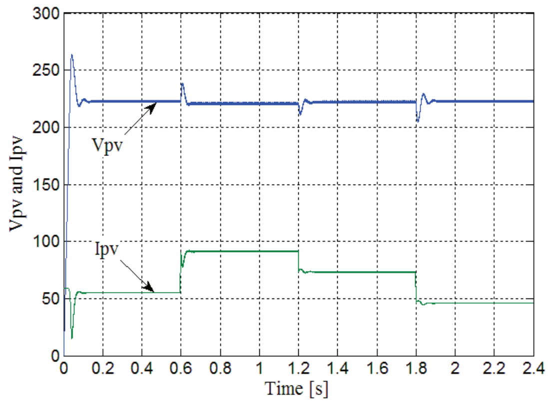

Fig. 7. PV array voltage (*Vpv*) and current (*Ipv*)

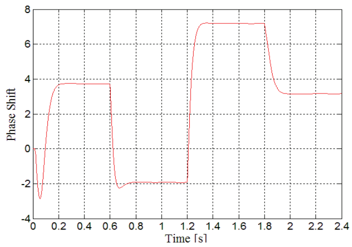

Fig. 8. Output voltage phase shift (δ)

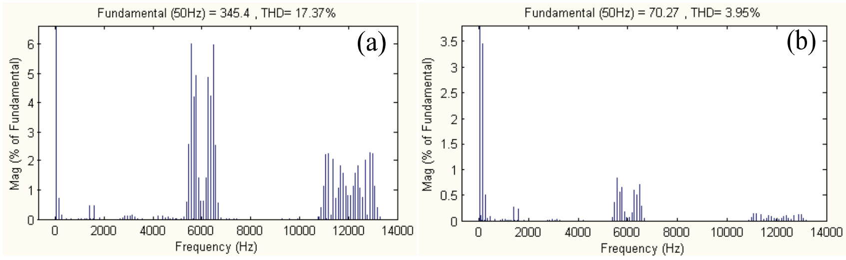

Fig. 9. Stage 1 Frequency spectrum for (a) Voltage waveform, (b) Current waveform

capacitor (Fig. 10) and flying capacitors (Fig. 11) to reach their target voltages. The PV output voltage, which has a filter capacitor, too, reaches to the maximum power point voltage in 0.1 sec (Fig. 7).

It is obvious that the control system tracks maximum power point of the PV array accurately with no any perturbation ($G_a = 600\,W/m^2$). Q_{ref} in this stage is zero, therefore, maximum power of the PV array injects to the grid with unity power factor. Fig. 12(a) shows the steady state waveforms of V_s, V_r and I (parameters are depicted in Fig. 4) in this condition. Finally the frequency spectrum of voltage and current waveforms are given in Fig. 9. Harmonic distortions are intensive in nkf_{sw}, where k is an integer number.

6.2. Stage 2: 0.6<t<1.2

At the second stage, Q_{ref} and irradiation level are increased to *15 kVar* and $1000\,W/m^2$, respectively. Fig. 12(b) shows the steady state waveforms in this stage. The frequency spectrum diagram is very similar to previous stage's, so extra explanation about that has been neglected, but all THD values of all stages for the steady state conditions are given in Table 5.

6.3. Stage 3: 1.2<t<1.8

This stage examines the most critical situation that can occur to the system because of the *19 kVar* change in reactive power reference. In this stage, the irradiation level of the PV array is decreased to $800\,W/m^2$. This stage is accomplished to only show the reactive power absorption capability of the system. As mentioned in Table 4, it takes 7 cycles (0.14 sec) for system to reach to *-4 kVar* reactive power. Fig. 12(c) depicts steady state waveforms in this stage. Total harmonic distortions for voltage and current waveforms in this stage are given in Table 5. Recall that Q_{ref} values for simulation are given in Table 6.

6.4. Stage 4: 1.8<t<2.4

In the fourth stage, the system reactive power and irradiation level are set to zero and $500\,W/m^2$, respectively. As mentioned in Table 4, system adapts this change in 9 cycles (0.18 sec). The steady state waveforms of the system are shown in Fig. 12(d). The voltage and current THD values are given in Table 5.

Table 4. The time to perform reactive power variation

Stage	Amount of change (kVar)	Cycles	Seconds
2	0 to 15	10	0.2
3	15 to -4	7	0.14
4	-4 to 0	9	0.18

Table 5. THD calculations for different stages

Stage	Start time (s)	No. of cycles	Voltage waveform THD (%)	Current waveform THD (%)
1	0.2	20	17.37	3.95
2	0.8	20	17.31	2.95
3	1.4	20	17.44	3.82
4	2.0	20	17.33	4.16

Table 6. Q_{ref} values

Stage	Time (s)	Q_{ref} (kVar)
1	0 - 0.6	0
2	0.6 - 1.2	15
3	1.2 - 1.8	-4
4	1.8 - 2.4	0

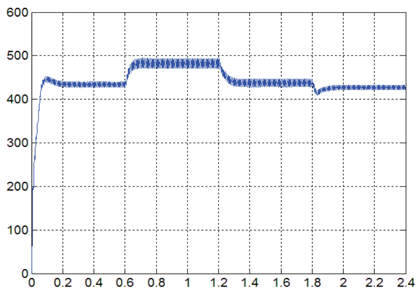

Fig. 10. Boost converter output voltage

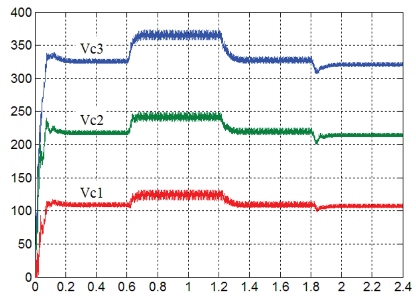

Fig. 11. Flying capacitors voltages

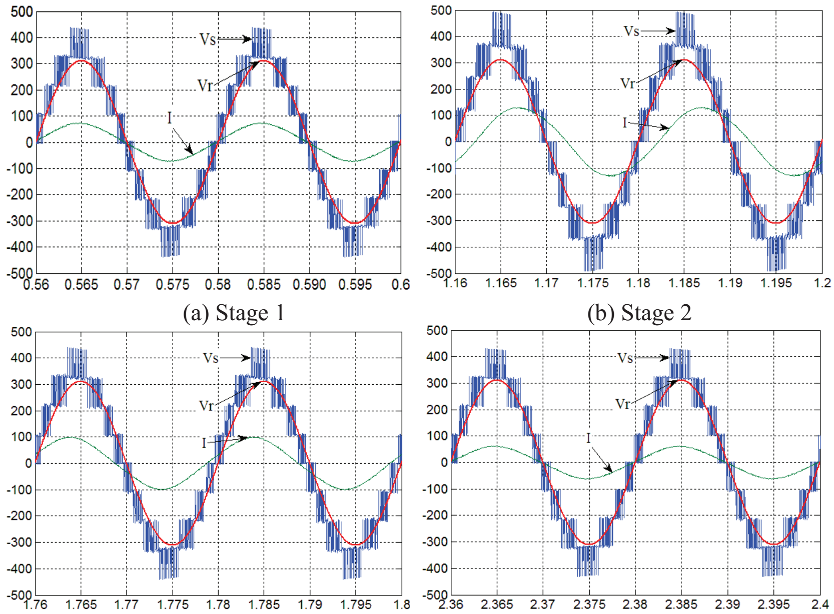

(a) Stage 1 (b) Stage 2

(c) Stage 3 (d) Stage 4

Fig. 12. The DFCM converter output voltage (*Vs*), Grid voltage behind the grid impedance (*Vr*), and the current injected to the grid (*I*)

7. Conclusions

In this paper, a new configuration of a PV generator with reactive power compensation capability was introduced. The proposed system employs two power electronics converters, that is, 1) a boost converter to operate the PV array at the maximum power point, and 2) a nine-level-DFCM converter which possesses various advantages in comparison with its counterparts. A robust control system has been developed, which can track the maximum power point of the PV array without any perturbation and control reactive power with a rapid response. In this system, the active and reactive power injection to the grid is independent, which means that regardless of the active power available from the PV array, any amount of reactive power can be injected to the grid. The proposed system developed, simulated, and analyzed in MATLAB software and the results demonstrate the system's performance. It is expected that the proposed system can be further studied via experimental results before implementation, whereas we are currently working toward a DSP based online controller including an efficient maximum power point tracker.

8. References

[1] H. L. Tsai, C. S. Tu, Y.J. Su, "Development of generalized photovoltaic model using MATLAB/SIMULINK", *Proceedings of the World Congress on Engineering and Computer Science (WCECS)*, San Francisco, CA, 2008.

[2] W. Nianchun, X. Qingshan, K. Yukita, Y. Goto, K. Ichiyanagi, A. Ueda, "Model of polycrystalline photovoltaic module in Matlab Simulink", *The Annual Meeting Record IEE*, Fukuoka, Japan, vol. 4, pp. 71-72, Mar, 2008.

[3] W. Nianchun, S. Zuo, K. Yukita, Y. Goto, K. Ichiyanagi, "Research of PV model and MPPT methods in Matlab" *IEEE Asia-Pacific Power and Energy Engineering Conference (APPEEC)*, Chengdu, China, 2010, pp. 1-4.

[4] F. M. G. Longatt, "Model of photovoltaic module in Matlab", *2do Congreso Iberoamericano de Estudiantes de Genieria Electrica Electronica y Computacion*, 2005.

[5] F. L. Tofoli, J. C. Schonell, C. A. Gallo, S. M. R. Sanhueza, "A low cost single-phase grid-connected photovoltaic system with reduced complexity" *IEEE Power Electronics Conference*, Bonito, Brazil, 2009, pp. 1033-1038.

[6] N. Abd Rahim, K. Chaniago, J. Selvaraj, "Single-phase seven-level grid-connected inverter for photovoltaic system", *IEEE Transactions on Industrial Electronics*, vol. 58, pp. 2435-2443, Mar, 2010.

[7] R. A. Mastromauro, M. Liserre, A. Dell'Aquila, "Single-phase grid-connected photovoltaic systems with power quality conditioner functionality", *IEEE European Conference on Power Electronics and Applications*, Alborg, Denmark, 2007, pp. 1-11.

[8] R. A. Mastromauro, M. Liserre, T. Kerekes, A. Dell'Aquila, "A single-phase voltage-controlled grid-connected photovoltaic system with power quality conditioner functionality", *IEEE Transactions on Industrial Electronics*, vol. 56, pp. 4436-4444, 2009.

[9] A. K. Sadigh, S. H. Hosseini, M. Sabahi, G. B. Gharehpetian, "Double flying capacitor multicell converter based on modified phase-shift pulsewidth modulation", *IEEE Transactions on Power Electronics*, vol. 25, pp. 1517-1526, Aug, 2010.

[10] M. Calais, V. G. Agelidis, "Multilevel converters for single-phase grid connected photovoltaic systems - an overview", *International Symposium on Industrial Electronics*, vol. 1, pp. 224-229, Jul, 1998.

[11] M. Calais, J. Myrzik, T. Spooner, V. G. Agelidis, "Inverters for single-phase grid connected photovoltaic systems - an overview", *IEEE 33rd Annual Power Electronics Specialists Conference*, vol. 4, pp. 1995-2000, Jun, 2002.

[12] S. B. Kjaer, J. K. Pedersen, F. Blaabjerg, "A review of single-phase grid-connected inverters for photovoltaic modules", *IEEE Transactions on Industry Applications*, vol. 41, pp. 1292-1306, Sept, 2005.